The origin and chemical evolution of carbon in the Galactic thin and thick discs[⋆]

T. Bensby[1]† and S. Feltzing[2]†

[1]*Department of Astronomy, University of Michigan, 830 Dennison Building, Ann Arbor, MI 48109-1042, USA*
[2]*Lund Observatory, Box 43, SE-221 00 Lund, Sweden*

ABSTRACT

In order to trace the origin and evolution of carbon in the Galactic disc, we have determined carbon abundances in 51 nearby F and G dwarf stars. The sample is divided into two kinematically distinct subsamples with 35 and 16 stars that are representative of the Galactic thin and thick discs, respectively. The analysis is based on spectral synthesis of the forbidden [C I] line at 872.7 nm using spectra of very high resolution ($R \approx 220\,000$) and high signal-to-noise ratio ($S/N \gtrsim 300$) that were obtained with the Coudé Echelle Spectrograph (CES) spectrograph by the European Southern Observatory (ESO) 3.6-m telescope at La Silla in Chile. We find that [C/Fe] versus [Fe/H] trends for the thin and thick discs are totally merged and flat for subsolar metallicities. The thin disc that extends to higher metallicities than the thick disc shows a shallow decline in [C/Fe] from [Fe/H] ≈ 0 and up to [Fe/H] $\approx +0.4$. The [C/O] versus [O/H] trends are well separated between the two discs (due to differences in the oxygen abundances) and bear a great resemblance to the [Fe/O] versus [O/H] trends. Our interpretation of our abundance trends is that the sources that are responsible for the carbon enrichment in the Galactic thin and thick discs have operated on a time-scale very similar to those that are responsible for the Fe and Y enrichment [i.e. SN Ia and asymptotic giant branch (AGB) stars, respectively]. We further note that there exist other observational data in the literature that favour massive stars as the main sources for carbon. In order to match our carbon trends, we believe that the carbon yields from massive stars then must be very dependent on metallicity for the C, Fe and Y trends to be so finely tuned in the two disc populations. Such metallicity-dependent yields are no longer supported by the new stellar models in the recent literature. For the Galaxy, we hence conclude that the carbon enrichment at metallicities typical of the disc is mainly due to low- and intermediate-mass stars, while massive stars are still the main carbon contributor at low metallicities (halo and metal-poor thick disc).

Key words: stars: abundances – stars: kinematics – Galaxy: abundances – Galaxy: disc – Galaxy: evolution.

1 INTRODUCTION

Next to hydrogen, helium and oxygen, carbon is the most abundant element in the Universe and plays an important role in the chemical evolution of galaxies. Although the nuclear process (helium burning) that is responsible for the formation of carbon atoms is well known (see e.g. reviews by Wallerstein et al. 1997; Arnett 2004), it is unclear that which objects contribute to the carbon enrichment of the interstellar medium. This has been much debated during recent years. Gustafsson et al. (1999) conclude that carbon is mainly contributed from massive, metal-rich stars, and not from low-mass stars. Chiappini, Romano & Matteucci (2003a) and Chiappini, Matteucci & Meynet (2003b) find strong indications that carbon is produced in low- and intermediate-mass stars. Shi, Zhao & Chen (2002) find that carbon is contributed by super-winds from massive stars in the early stages of disc formation in the Galaxy, while at later stages significant amount of carbon is contributed by low-mass stars. Other studies that favour a mixture of low-, intermediate- and high-mass stars include Liang, Zhao & Shi (2001); Gavilán, Buell & Mollá (2005) and Carigi et al. (2005) while Henry, Kwitter & Bates (2000) and Akerman et al. (2004) suggest massive stars to be the main source.

Only a few previous studies (Andersson & Edvardsson 1994; Gustafsson et al. 1999; Takeda & Honda 2005) have based their carbon abundances on the forbidden [C I] line at 872.7 nm. This line is highly insensitive to errors in the stellar model atmosphere (see e.g. Asplund et al. 2005) and gives carbon abundances of high accuracy in solar-type stars, even when using one-dimensional (1D) models under the assumption of local thermodynamic equilibrium (LTE). Unfortunately, the line is very weak and is blended with a weak feature that is likely to be an Fe I line (e.g. Lambert & Swings 1967). So, in order to achieve accurate abundances from this line, it is desirable to have spectra of high-resolution and high signal-to-noise ratio (S/N), and it is essentially only the Gustafsson et al. (1999) study that has reliable carbon trends based on the forbidden line (see discussion in Section 4.5). They did, however, not include the blending Fe I line in their analysis.

As a step to achieve a deeper understanding of the sites of carbon formation and the chemical histories of the Galactic discs, we have obtained high-resolution, high S/N spectra of the forbidden [C I] line at 872.7 nm for 51 dwarf stars in the solar neighbourhood. These stars are already well studied, have well-determined oxygen and iron abundances and have known kinematics (Bensby, Feltzing & Lundström 2003, 2004; Bensby et al. 2005). The fact that the kinematics are known is important as this makes it possible to properly investigate the carbon trends in the two discs, independent of each other, and to perform a differential analysis of the carbon trends in the thin and thick discs in order to investigate the differences and similarities in the discs' chemical histories. The latter investigation could, combined with other evidence, be important for understanding the time-scales involved in the chemical enrichment of the gas that today make up what we observe as the stars in the Galactic thick disc.

In Section 2, we shortly describe the stellar sample and the observations. Section 3 discusses the data reduction and associated problems, and Section 4 discusses the abundance analysis and estimate random and systematic errors in the derived carbon abundances. In Section 5, we describe our resulting carbon trends and use our results to trace the possible sources of carbon as well as discuss the chemical evolution of the Galactic discs. Finally, Section 6 concludes with a summary of our findings.

2 STELLAR SAMPLE AND OBSERVATIONS

The stellar sample (listed in Table 1) contains 51 F and G dwarf stars (35 thin disc and 16 thick disc stars) which form a subset of the samples in our previous studies (in total 102 stars; see Bensby et al. 2003, 2004, 2005). The selection criteria used to assign a star to either the thin or the thick disc as well as further details and discussions about the kinematic properties of the stars in the sample can be found in Bensby et al. (2003, 2005) and in Section 5.1.

Observations were carried out by TB during six nights in 2004 September with the Coudé Echelle Spectrograph (CES) by ESO 3.6-m telescope in La Silla in Chile. All spectra were obtained with the highest resolution $R \approx 220\,000$. Although our exposure times were calculated to give spectra with S/N that exceeds at least 350, this was unfortunately rarely the case in the reduced spectra. The reason for this degradation in quality of the reduced spectra is due to unexpectedly strong fringing patterns from/in the CCD detector in this wavelength region. The treatment of this feature is discussed in more detail in Section 3.

Furthermore, long exposures were split into shorter exposures of maximum 30 min. Solar spectra were obtained on each day by observing the day-sky approximately 1 h before sunset. Flat-field

and bias exposures were taken at the beginning and at the end of the nights, and additional flat-fields at least once more during the nights. Wavelength calibration spectra were obtained from a thorium–argon hollow cathode lamp. On the last four nights, we also included exposures of rapidly rotating B stars that were used in the reduction procedure to minimize the residuals from the fringing pattern.

3 DATA REDUCTION

The top panel in Fig. 1 shows a part of the CCD frame for a (normalized) flat-field exposure and the middle panel, a solar spectrum. As can be seen, they are severely affected by fringing. However, this fringing pattern was stable and did not change over the six nights during which the observations lasted. As the removal of this pattern is extremely important for the quality of our results, we give a more detailed description of the reduction process.

The spectra were reduced using standard routines in the MIDAS[1] software package and consisted of the following steps.

(i) One master bias frame and several (typically four to five) master flat-field frames were constructed for each of the six nights by averaging multiple exposures. Bias subtraction for the flat-fields was done after the bias value had been corrected for the difference between its overscan value and that of the flat-field frame. Since the main method for removing fringing patterns is through the flat-fielding process, care was taken when normalizing the flat-field frames. As proposed to be the best method in the CES manual,[2] we normalized the flat-field row by row, i.e. a low-order polynomial was fitted to each row (i.e. along the dispersion direction) in the flat-field frame. This process is necessary since the flat-fields are obtained through the fibre and the image slicer which results in a flat-field profile that is composed of the same 12 slices as the science exposures (see Fig. 2). A plain division by this 'non-flat' flat-field would result in too high weights given to the low-flux minima regions between the slices (i.e. dividing low numbers by low numbers). A normalized flat-field frame can be seen in the top panel in Fig. 1.

(ii) The science frames were first corrected for the bias level. Before dividing by a flat-field frame, we also corrected the frames for the fact that the background level is higher on the right-hand side than on the left-hand side of the profile perpendicular to the dispersion direction (see Fig. 2). This is due to scattered light originating within the CES and does not contribute to the fringing pattern. If it is not corrected for before the flat-fielding, the division by the flat-field will overcompensate the pattern. We therefore fitted linear functions between the left-hand side (approximate pixel number 400) and the right-hand side (approximate pixel number 800) and made a subtraction so that the two sides were level. This correction had a very positive effect on the quality of the reduced spectra for stars with long exposure times as the difference between the two sides relative to the total flux of the object seems to increase with exposure time. For the flat-field exposures, the difference between left- and right-hand sides is practically zero. After this correction, we divided the science frames with the normalized flat-field frames. The middle panel in Fig. 1 shows a 'raw' science frame and the bottom panel in Fig. 1 an example of a frame that has been corrected for the straylight pedestal and then divided by the normalized

---

Table 1. Stellar names, chemical abundances and stellar parameters. Abundances are given relative to our solar abundances. [C/H] abundances derived without the blending Fe I line are given in italics in parentheses. Metallicities ([Fe/H]), effective temperatures ($T_{\rm eff}$), surface gravities (log g), microturbulences ($\xi_{\rm t}$) and space velocities ($U_{\rm LSR}$, $V_{\rm LSR}$, $W_{\rm LSR}$) are taken from Bensby et al. (2003, 2005). Oxygen abundances ([O/H]) are taken from Bensby et al. (2004b) and are generally based on the forbidden [O I] line at 630.0 nm unless otherwise indicated ('*' means that the permitted O I triplet lines at λ ≈ 777 nm were used and '**' means that the forbidden [O I] line at λ = 636.3 nm was used). $v_{\rm R-T}$ is the macroturbulent broadening (RAD–TAN) that we used (these values have no 'real physical' meaning and are only listed for completeness).

| HIP	HD	[Fe/H]	[C/H]	([C/H])	[O/H]	[C/O]	$T_{\rm eff}$ [K]	log g (CGS)	$\xi_{\rm t}$ (km s^{-1})	$v_{\rm R-T}$ (km s^{-1})	$U_{\rm LSR}$ (km s^{-1})	$V_{\rm LSR}$ (km s^{-1})	$W_{\rm LSR}$ (km s^{-1})
						Thin disk stars							
910	693	−0.36	−0.33	(−0.34)			6220	4.07	1.43	5.09	29.0	−7.8	−11.1
2235	2454	−0.28	−0.11	(−0.13)			6645	4.17	1.75	8.33	23.2	−26.2	−6.7
2787	3229	−0.11	−0.05	(−0.08)			6620	3.86	1.70	5.44	−16.5	−21.7	−12.9
3142	3735	−0.45	−0.37	(−0.39)	−0.25	−0.12	6100	4.07	1.50	4.13	−35.5	−45.8	19.9
3909	4813	−0.06	−0.02	(−0.03)	−0.11	0.09	6270	4.41	1.12	3.85	31.4	2.5	−4.8
5862	7570	0.17	0.21	(0.20)	0.06	0.15	6100	4.26	1.10	4.96	−34.1	−17.1	−6.0
7276	9562	0.20	0.19	(0.18)	0.14	0.05	5930	3.99	1.35	4.38	1.1	−21.1	19.5
9085	12042	−0.31	−0.20	(−0.22)	*−0.12	−0.08	6200	4.25	1.30	5.43	−42.5	−5.1	1.0
10306	13555	−0.17	−0.03	(−0.05)			6560	4.04	1.75	8.20	−10.3	−6.8	11.2
12611	17006	0.26	0.18	(0.22)	**0.14	0.04	5250	3.66	1.35	3.47	22.0	−13.5	0.1
12653	17051	0.14	0.15	(0.14)	0.04	0.11	6150	4.37	1.25	6.67	−21.3	−12.8	−3.1
14954	19994	0.19	0.21	(0.20)	0.11	0.10	6240	4.10	1.60	9.24	−9.7	−14.2	1.2
15131	20407	−0.52	−0.39	(−0.40)	−0.26	−0.13	5834	4.35	1.00	2.97	3.6	20.2	−9.6
17378	23249	0.24	0.10	(0.18)	0.13	−0.03	5020	3.73	0.80	3.15	−4.8	31.6	18.5
23941	33256	−0.30	−0.20	(−0.22)	*−0.23	0.03	6427	4.04	1.90	10.0	−2.0	−1.9	8.1
24829	35072	0.06	0.09	(0.07)	0.03	0.06	6360	3.93	1.70	4.45	−36.8	−26.3	−15.5
29271	43834	0.10	0.08	(0.11)	0.02	0.06	5550	4.38	0.80	2.63	29.5	−27.2	−5.8
78955	144585	0.33	0.21	(0.22)	0.17	0.04	5880	4.22	1.12	3.16	−16.6	−16.2	25.4
80337	147513	0.03	−0.09	(−0.07)	0.03	−0.12	5880	4.49	1.10	3.08	24.0	4.0	5.8
80686	147584	−0.06	−0.13	(−0.13)	−0.05	−0.08	6090	4.45	1.01	3.99	18.5	14.3	2.5
84551	156098	0.12	0.07	(0.05)	0.12	−0.05	6475	3.79	2.00	7.61	−31.9	−14.7	16.8
84636	156365	0.23	0.21	(0.21)	0.15	0.06	5820	3.91	1.30	4.18	1.7	3.8	−21.4
86796	160691	0.32	0.25	(0.26)	0.14	0.11	5800	4.30	1.05	3.44	−5.0	−2.7	3.5
87523	162396	−0.40	−0.33	(−0.35)	−0.31	−0.02	6070	4.07	1.36	3.72	−14.9	−5.2	−23.7
90485	169830	0.12	0.18	(0.17)	**0.06	0.12	6339	4.05	1.55	4.42	−6.1	6.5	10.9
91438	172051	−0.24	−0.30	(−0.28)	−0.18	−0.12	5580	4.42	0.55	2.27	47.1	3.0	2.9
99240	190248	0.37	0.25	(0.29)	0.19	0.24	5585	4.26	0.98	3.08	−38.2	−8.5	−8.2
103682	199960	0.27	0.25	(0.25)	0.14	0.11	5940	4.26	1.25	3.70	3.8	−18.1	3.6
105858	203608	−0.73	−0.60	(−0.62)	−0.46	−0.14	6067	4.27	1.17	3.50	−3.8	49.5	13.7
109378	210277	0.22	0.10	(0.15)	0.16	−0.06	5500	4.30	0.78	2.60	13.6	−45.5	1.8
110341	211976	−0.17	−0.14	(−0.15)	−0.11	−0.03	6500	4.29	1.70	6.64	4.7	11.5	0.7
113137	216437	0.22	0.22	(0.22)	0.13	−0.09	5800	4.10	1.16	3.99	14.1	15.0	5.2
113357	217014	0.20	0.13	(0.15)	0.10	0.03	5789	4.34	1.00	3.23	−5.2	−23.2	22.0
113421	217107	0.35	0.27	(0.31)	0.16	0.11	5620	4.29	0.97	2.75	8.3	−3.8	18.3
117880	224022	0.12	0.19	(0.17)	0.05	0.14	6100	4.21	1.30	5.36	−36.2	−11.4	2.8
						Thick disk stars							
3086	3628	−0.11	0.04	(0.03)	0.09	−0.05	5840	4.15	1.15	2.99	−159.4	−48.4	53.6
3497	4308	−0.33	−0.25	(−0.25)	−0.05	−0.20	5636	4.30	0.80	2.97	60.0	−103.7	−19.0
5315	6734	−0.42	−0.42	(−0.38)	0.00	−0.42	5030	3.46	0.86	2.41	60.3	−118.0	46.3
14086	18907	−0.59	−0.53	(−0.52)	−0.16	−0.37	5110	3.51	0.87	2.54	18.6	−78.1	−13.1
15510	20794	−0.41	−0.38	(−0.35)	−0.01	−0.37	5480	4.43	0.75	2.04	−69.4	−89.3	−24.0
17147	22879	−0.84	−0.76	(−0.77)	−0.32	−0.44	5920	4.33	1.20	2.29	−99.0	−80.4	−37.0
18235	24616	−0.71	−0.72	(−0.71)	−0.24	−0.48	5000	3.13	0.95	2.97	−17.0	−158.1	−20.1
75181	136352	−0.34	−0.20	(−0.21)	0.00	−0.20	5650	4.30	0.78	2.58	−109.5	−41.4	43.3
79137	145148	0.30	0.12	(0.24)	0.20	−0.08	4900	3.62	0.60	3.03	81.5	−49.8	−62.6
82588	152391	−0.02	−0.11	(−0.02)	0.01	−0.12	5470	4.55	0.90	3.32	94.1	−105.5	16.6
88622	165401	−0.46	−0.44	(−0.44)	−0.05	−0.39	5720	4.35	0.80	3.17	−68.6	−84.7	−31.7
96124	183877	−0.20	−0.07	(−0.06)	0.08	−0.15	5590	4.37	0.78	2.27	−28.0	−87.4	−15.4
103458	199288	−0.65	−0.56	(−0.57)	−0.29	−0.27	5780	4.30	0.90	2.60	31.3	−96.3	52.9
108736	208998	−0.38	−0.30	(−0.31)	−0.01	−0.29	5890	4.24	1.05	3.00	−15.6	−72.9	44.6
109821	210918	−0.08	−0.08	(−0.08)	0.10	−0.18	5800	4.29	1.05	2.72	−36.9	−86.9	−2.5
118115	224383	−0.01	0.07	(0.07)	0.04	0.03	5800	4.30	1.00	3.05	−65.0	−77.9	3.3
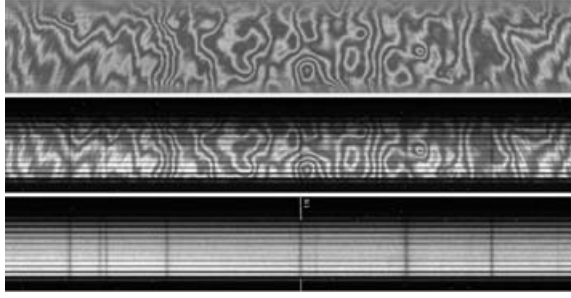
Figure 1. Top: a normalized flat-field frame. Middle: a 'raw' science frame (in this case a solar spectrum) Lower: the flat-fielded science frame. The strong Si I line at 872.8 nm, in whose left wing the [C I] line is located, has been marked. The full CCD frames are 4096 × 1024 pixel. Here, we show the central parts (approximately 2000× 500 pixels in size) from ∼871.6 to ∼874.0 nm.
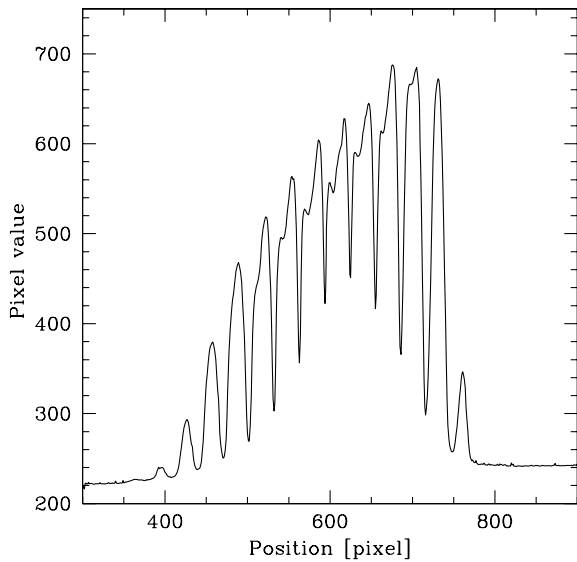

Figure 2. The average profile (based on 4096 rows) perpendicular to the dispersion direction. Note that the background level is higher on the right-hand side (pixel value ∼240) than on the left-hand side (pixel value ∼220).

flat-field frame shown in the top panel in Fig. 1. In this way, we were quite efficiently able to remove much of the fringing pattern which is further illustrated in Fig. 3. The final spectra were also filtered for cosmic ray hits (using the MIDAS task FILTER/COSMIC) before dividing with the flat-field.

(iii) 1D spectra were obtained by summing the fluxes of all 12 slices (including the regions in between the slices; see Fig. 2). The spectra were then wavelength calibrated and re-binned to constant steps in wavelength. Fig. 3 shows the reduced solar spectrum.

(iv) We also observed several rapidly rotating B stars. Since their spectral lines are all smeared out, their spectra should more or less form a featureless continuum. However, the reduced spectra for our 19 B stars have a structure that shows very little variance when compared to each other (apart from variations in the S/N). This makes it most likely that this structure is the remains of an 'imperfect' removal of the fringing and what we see in the B star spectra should without any doubt also be present in all our other reduced spectra. In order to further reduce the residuals from the fringing, we therefore divided all spectra with a normalized B star template. This B star template was derived as a weighted average of all 19 B star spectra.
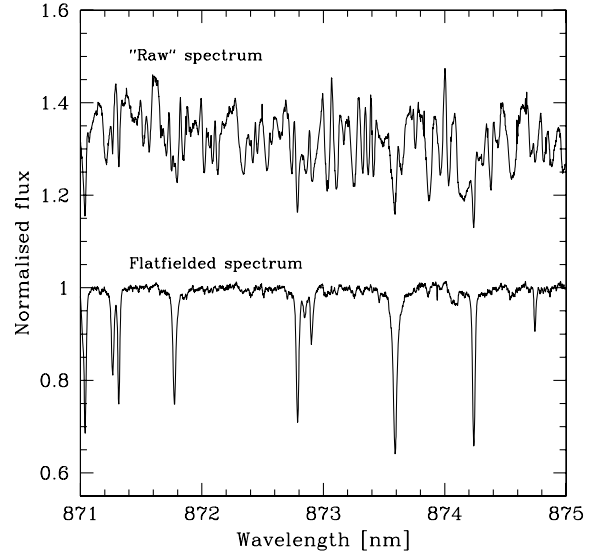

Figure 3. This comparison shows the efficiency of the flat-field in removing the fringing pattern from a 'raw' image. The 1D spectra shown here are the same as those in the two bottom panels in Fig. 1 with the exception that the reduced and flat-fielded spectrum has been filtered for cosmic ray hits (which was not the case in Fig. 1). The 'raw' spectrum has also been normalized and vertically shifted for this plot.
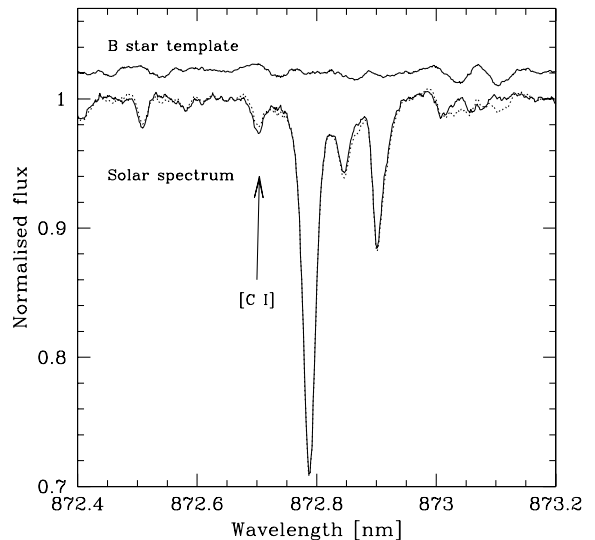

Figure 4. The top spectrum shows the B star template. It has been shifted vertically for this plot. Also shown is a reduced solar spectrum (dotted line, same spectrum as in Fig. 3) and the same solar spectrum but divided by the normalized B star template (solid line).

Fig. 4 shows the normalized B star template and the solar spectrum before and after division with it.

(v) For stars that have multiple exposures, we then co-added the individual spectra to one spectrum. Finally, the spectra were normalized by fitting a low-order Legendre polynomial to the continuum using the IRAF[3] task CONTINUUM.

[3] IRAF is distributed by National Optical Astronomy Observatories, operated by the Association of Universities for Research in Astronomy, Inc., under contract with the National Science Foundation, USA.

4 ABUNDANCE DETERMINATION

4.1 Stellar atmospheres

We use 1D, plane-parallel LTE stellar model atmospheres that were calculated with the Uppsala MARCS code (Gustafsson et al. 1975; Edvardsson et al. 1993; Asplund et al. 1997). Surface gravities ($\log g$) were determined from *Hipparcos* parallaxes, metallicities ([Fe/H]) were determined using Fe I lines, effective temperatures (T_{eff}) were determined by requiring that the abundances derived from Fe I lines with different excitation energies should all yield the same [Fe/H] and the microturbulence parameter (ξ_t) by requiring all Fe I lines should yield the same abundances independent of line strength ($\log W_\lambda/\lambda$). All these parameters (listed in Table 1) were determined in our previous studies (Bensby et al. 2003, 2005) wherein the iterative process to tune the stellar parameters is also fully described.

The [Fe/H] values listed in Table 1 are given relative to the solar Fe abundance that we derived using solar spectra obtained with the same spectrographs as the stellar spectra (see Bensby et al. 2003, 2005). In these studies, we also compare our derived [Fe/H] values as derived from Fe I lines to the [Fe/H] values derived from Fe II lines (these we did not use in the tuning of the stellar parameters). Fe II lines are more robust indicators than Fe I lines (see Asplund 2005) since they are normally not affected by departures from LTE. As we generally find good agreement between the [Fe/H] values derived from Fe I and Fe II lines, respectively (see fig. 7 in Bensby et al. 2003, and fig. 2 in Bensby et al. 2005), this indicates that for the range of parameters that the stars in our investigations span the effects of departures from LTE are small, if at all measurable.

4.2 Synthetic spectra, atomic data and line broadening

The synthetic spectra were calculated with the Uppsala SPECTRUM software. As input, it needs a stellar atmosphere model and a list of spectral lines with atomic data. To properly reproduce the region around the [C I] line, we used the Vienna Atomic Line Database (VALD; Piskunov et al. 1995; Kupka et al. 1999; Ryabchikova et al. 1999) to extract all lines in the region 872.0–873.5 nm. Table 2 lists the atomic data for the [C I] line at 872.7126 nm ($\log gf = -8.136$, theoretical from Hibbert et al. 1993; Galavis, Mendoza & Zeippen 1997), the blending Fe I line at 872.7132 nm ($\log gf = -3.93$, theoretical from Kurucz 1993) and the Si I line at 872.8010 nm ($\log gf = -0.42$,

Table 2. Atomic data. The columns give: element and ionisation stage, wavelength, lower excitation energy, $\log gf$-value, method for collisional broadening (see Section 4.2), correction factor to the classical Unsöld broadening, damping constants and references for the $\log gf$-values: H93 = Hibbert et al. (2003); G97 = Galavis et al. (1997); K93 = Kurucz (1993); BFL03 = Bensby et al. (2003). (Note: see discussion in Section 4.4 and in Allende Prieto et al. (2002) regarding the Fe I line and why $\log gf = -3.93$ is likely an overestimate). The full line list that was used in the calculations of the synthetic spectra can be reproduced by querying the VALD database (http://www.astro.uu.se/~vald) for lines in the region 872.0–873.5 nm.

	λ (nm)	χ_1 (eV)	$\log gf$	DMP	$\delta\gamma_6$	γ_{rad} (s^{-1})	Ref.
[C I]	872.7126	1.264	−8.136	U	2.50	1.0E+05	H93, G97
Fe I	872.7132	4.186	−3.930	U	1.40	6.1E+07	K93
Si I	872.8010	6.181	−0.42*	C		1.0E+05	BFL03

astrophysical from Bensby et al. 2003) whose left wing form the continuum level for the [C I] line.

The broadening of atomic lines by radiation damping was considered in the determination of the abundances, and the damping constants (γ_{rad}) for the different lines were taken from the VALD data base. Collisional broadening, or Van der Waals broadening, by hydrogen atoms was also considered. The width cross-section for the Si I line at 872.8010 nm is taken from Barklem, O'Mara & Ross (1998) (indicated by a 'C' in Table 2), and for the other two lines we apply the correction term ($\delta\gamma_6$) to the classical Unsöld approximation for the Van der Waals damping (indicated by a 'U' in Table 2).

The synthetic spectrum is then convolved with a line profile to reproduce the instrumental broadening and then with another line profile to reproduce the broadening due to large-scale motions in the stellar atmosphere. The width of the instrument broadening profile is set by the resolution of the spectra, and in our case it was 0.0042 nm. This value was determined by measuring the full width at half-maximums (FWHMs) in the Th–Ar spectra and corresponds to a spectral resolving power of about $R \sim 208\,000$ at 873.0 nm ($R \equiv \lambda/\Delta\lambda = 873.0/0.0042$). The large-scale motions include macroturbulence (that has a radial–tangential, 'RAD–TAN', profile) as well as the line-of-sight component ($v\sin i$) of the stellar rotational velocity. The contribution from $v\sin i$ is usually small in our types of stars (F and G dwarf stars) in comparison to the macroturbulence (see e.g. Gray 1992). To determine the widths of the RAD–TAN profiles, we used the quite strong Si I line at 872.8 nm. First, we usually had to change the $\log gf$-value of the Si I line in order to get the line strength correct. We then made 20 different synthetic spectra with different RAD–TAN broadenings from 0 to 10 km s^{-1}. The best fit was found by minimizing an unnormalized χ^2-function. Here, as we only want to find the best solution with a given set of free parameters, we need not normalize our χ^2s. An example of this is shown in Fig. 5.
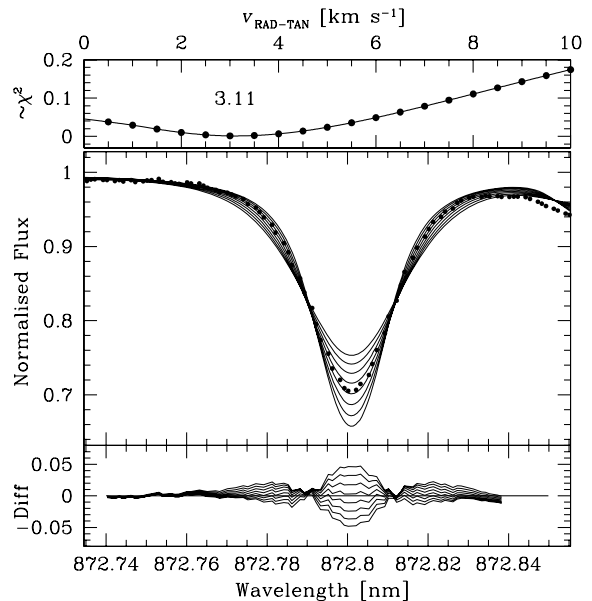

Figure 5. Determination of the broadening due to macroturbulence (see Section 4.2). This plot shows the solar spectrum for which we found a best matching RAD–TAN profile with a width of 3.11 km s^{-1}. The synthetic spectra shown in the two bottom panels have RAD–TAN widths from 1.5 to 5.0 km s^{-1}.

4.3 Carbon abundances

The forbidden carbon line is located in the left wing of a Si I line and is blended by a line that is most likely an Fe I line (Lambert & Swings 1967). The contribution from this blending line to the joint [C I]-Fe I line profile is generally negligible at subsolar metallicities, while in the Sun it is estimated to be between 0.1 pm and 0.5 pm (Allende Prieto, Lambert & Asplund 2002). While most previous studies have chosen to neglect this line in their abundance analyses due to its assumed weakness and uncertain atomic data, we have included it as our sample contains many stars at super-solar [Fe/H] where such a blend will grow in size. Since this Fe I line only has a calculated $\log gf$-value (Kurucz 1993), and could therefore be associated with large errors, we must be careful and make extensive checks. For comparison purposes, we will therefore also determine carbon abundances neglecting the Fe I blend.

By producing a set of synthetic spectra with carbon abundances varying in steps of 0.03 dex, we then minimized an unnormalized χ^2-function to find the best-fitting synthetic spectrum and hence the carbon abundance (in the same way as we determined the macroturbulence broadening; see Fig. 5). For seven stars (HIP 10798, 72673, 81520, 102264, 107975, 3185 and 109450), we did not determine carbon abundances because their spectra showed defects probably as a result of an insufficient removal of the fringing pattern.

Fig. 6 shows an example of the observed and the synthetic spectra for the Sun. From our analysis of the solar spectrum (using a MARCS model atmosphere with $T_{eff} = 5777$ K, $\log g = 4.44$, $\xi_t = 0.85$ km s^{-1} and RAD–TAN profile of 3.11 km s^{-1}; see Fig. 5), we get a solar carbon abundance of $\log \epsilon_\odot(C)$ 8.41 when the blending Fe I line is taken into account and $\log \epsilon_\odot(C) = 8.44$ when it is neglected. Both are in good agreement with the recent analysis by Allende Prieto et al. (2002) and Asplund et al. (2005) who found a best value of $\log \epsilon_\odot(C) = 8.39$ using 3D stellar atmosphere models and $\log \epsilon_\odot(C) = 8.41$ when using a MARCS model atmosphere. These studies did, however, not include the blending Fe I line in their calculations. The reason that we see a difference of 0.03 dex (8.44–
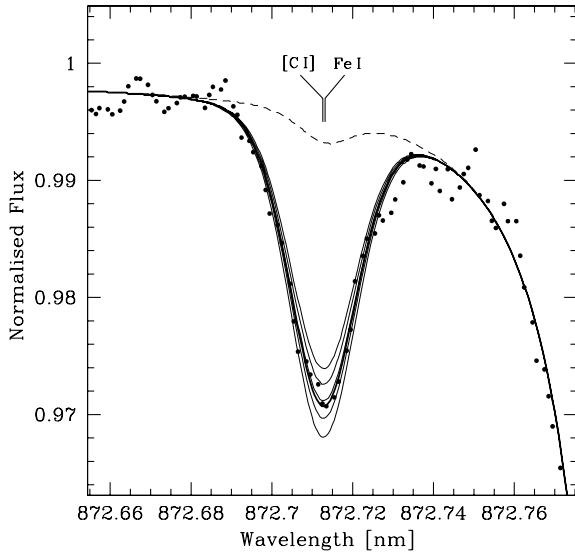
8.41) between our and Allende Prieto et al. (2002) analysis, both using MARCS atmosphere models, is probably due to uncertainties in the placement of the continuum and/or differences between the spectra (that could originate from the data reduction process; see Section 3).

Our final [C/H] abundances, both with and without the Fe I blend taken into account, are listed in Table 1 [given relative to our solar abundance $\log \epsilon_\odot(C) = 8.41$ and $\log \epsilon_\odot(C) = 8.44$, respectively].

4.4 Fe I blend or no Fe I blend?

How does the inclusion of the Fe I blend influence our final carbon abundances and carbon trends? In Figs 7(a)–(c), we show the difference in [C/H] versus T_{eff}, $\log g$ and [Fe/H], respectively. There is a clear trend with T_{eff}; the lower the temperature the larger is the effect on [C/H] when neglecting the blend. The reason that the difference in [C/H] generally is negative below 5700 K and positive at higher temperatures is because our abundance analysis is differential to the Sun. At effective temperatures higher than $\sim$5700 K, the difference in [C/H] is always smaller than $\sim$0.03 dex no matter if the stars have high or low metallicities. No absolute trend with [Fe/H] can be seen (there is still a number of stars at high metallicities where the difference is negligible). From this, we conclude that it is for a combination of low T_{eff} (and often low $\log g$) and high [Fe/H] that we need to be extra careful and correctly include the Fe I blend.

In Figs 7(d)–(e), we show the effect of the Fe I blend on the final [C/Fe] versus [Fe/H] trend. Apart from a somewhat lower spread in [C/Fe], when neglecting the blend the trends are essentially identical: both have a flat [C/Fe] trend at [Fe/H] < 0 and at [Fe/H] > 0 the [C/Fe] ratio declines when going to higher metallicities. Fig. 7(f) shows the trend (derived *with* the blend) but for stars that have $T_{eff} > 5700$ K and for which the effect on [C/Fe] due to an erroneous treatment of the blend should be minimal [see Fig. 7(a)]. The trend seen in Figs 7(d)–(e) still persists.

In Summary, we conclude that it is important to include the Fe I blend for stars that have low effective temperatures (below 5700 K) and then especially at high [Fe/H]. It is, however, important to remember that the $\log gf$-value that is available for the Fe I line is a theoretical one (Kurucz 1993), and it is possible that the calculated line strength for the blend is either over- or underestimated. It would therefore be very valuable to have an accurate experimental $\log gf$-value for this Fe I line so that it is possible to properly calculate its contribution to the joint [C I]-Fe I line profile. We note that Lambert & Ries (1977) tried to estimate the $\log gf$-value for this line by ensuring that the same C abundance is derived from the [C I] line as from C_2 and CH lines. They arrived at a value of $\log gf \approx -3.6$ which would lead to a higher Fe I contribution to the joint [C I] - Fe I line profile at 872.7 nm than indicated by $\log gf = -3.93$ from Kurucz (1993). By looking at other Fe I lines belonging to the same multiplet, Allende Prieto et al. (2002) concluded in their analysis of the solar spectrum that the contribution should be significantly lower and hence that $\log gf = -3.93$ would overestimate the line strength of the blending Fe I line. The conclusion of Allende Prieto et al. (2002) means that our carbon abundances might be somewhat underestimated at high [Fe/H] since we used $\log gf = -3.93$ from Kurucz (1993). However, for our stellar sample we see that the general appearance of the [C/Fe] versus [Fe/H] trend is not affected by the blend (apart from a somewhat smaller spread in [C/Fe] when *neglecting* it). In what follows, we therefore continue to use our carbon abundances that we derived *with* the Fe I blend, and these are the values we hereafter refer to unless otherwise indicated.
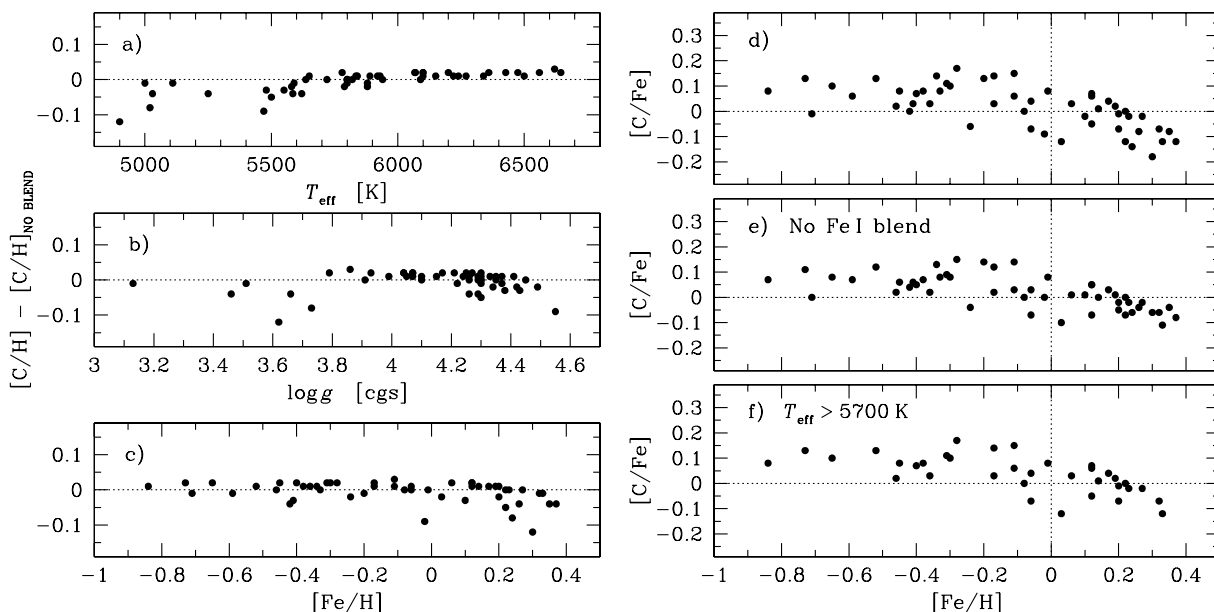

Figure 6. The [C I] line in the solar spectrum. The dots are the observed spectrum and the *thick* solid line the best fit representing a solar carbon abundance of $\log \epsilon_\odot(C) = 8.41$. The thin solid lines represent five different carbon abundances from 8.34 to 8.46 dex in steps of 0.03 dex. The dashed line shows the contribution from the blending Fe I line. The wavelength positions of the [C I] and the Fe I lines are also indicated.

Figure 7. The effect on [C/H] when not including the Fe I blend when synthesizing the [C I] line. The difference between the two derivations of carbon is shown in (a) versus effective temperature; (b) versus surface gravity and (c) versus metallicity. Fig. (d) shows the [C/Fe] versus [Fe/H] trend for all stars; (e) [C/Fe] versus [Fe/H] for all stars when neglecting the Fe I blend and (f) [C/Fe] versus [Fe/H] (when including the Fe I blend) for stars that have $T_{\rm eff} > 5700\,{\rm K}$.
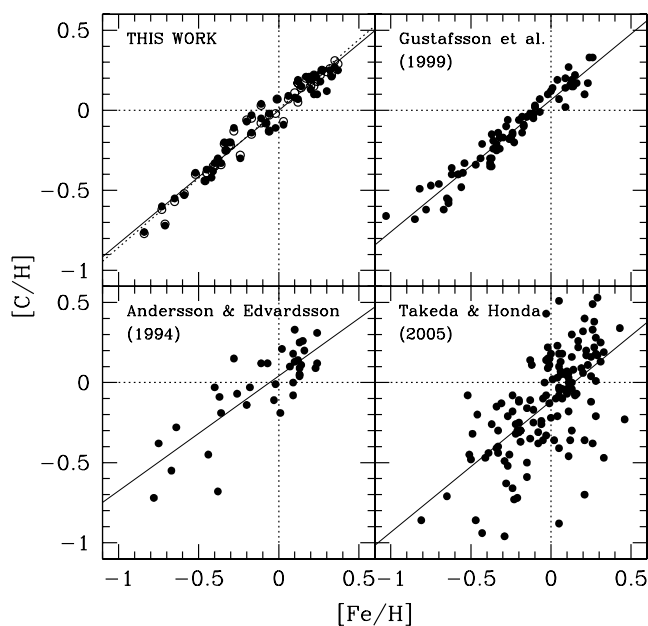

Figure 8. [C/H] versus [Fe/H] for our and the stellar samples from Gustafsson et al. (1999), Andersson & Edvardsson (1994) and Takeda & Honda (2005). Linear regression lines are also plotted, see equations (1)–(5). For our stellar sample, we also plot the abundances that were derived when neglecting the Fe I blend (open circles and dotted line).

4.5 Error analysis

To check for systematic effects, we compare our derived carbon abundances to other studies that also use the forbidden [C I] line as indicator of the carbon abundance (Andersson & Edvardsson 1994; Gustafsson et al. 1999; Takeda & Honda 2005). In Fig. 8, we plot [C/H] versus [Fe/H] for our data set as well as for data from these three studies. For each data set, we have done a simple linear re-

gression between [C/H] and [Fe/H]. These are overplotted in Fig. 8. The regression lines are given by the following equations (where G99 = Gustafsson et al. 1999; AE94 = Andersson & Edvardsson 1994; TH05 = Takeda & Honda 2005):

$$[{\rm C/H}] = [{\rm Fe/H}]0.83 - 0.00 \quad {\rm (this\ work)}, \tag{1}$$

$$[{\rm C/H}] = [{\rm Fe/H}]0.87 + 0.01 \quad {\rm (this\ work,\ no\ blend)}, \tag{2}$$

$$[{\rm C/H}] = [{\rm Fe/H}]0.82 + 0.07 \quad {\rm (G99)}, \tag{3}$$

$$[{\rm C/H}] = [{\rm Fe/H}]0.72 + 0.04 \quad {\rm (AE94)}, \tag{4}$$

$$[{\rm C/H}] = [{\rm Fe/H}]0.82 - 0.12 \quad {\rm (TH05)}. \tag{5}$$

The tight relation between [C/H] and [Fe/H] that we see for our stellar sample (see Fig. 8) is also present in the Gustafsson et al. (1999) data set (see also their fig. 3). As can be seen, the slopes (Δ[C/H]/Δ[Fe/H]) are essentially the same for our stellar sample and the Gustafsson et al. (1999) and Takeda & Honda (2005) samples. There are, however, offsets present between these two data sets and ours. Relative to our relationship, the Gustafsson et al. (1999) relationship is shifted 0.07-dex upwards (to higher [C/H] values) while the Takeda & Honda (2005) relationship is shifted 0.12-dex downwards (to lower [C/H] values). The relationship from the Andersson & Edvardsson (1994) data set[4] is shifted upwards by 0.04 dex relative to our relationship and differs from the other three in that it shows a shallower slope. The Andersson & Edvardsson (1994) and Takeda & Honda (2005) data sets have a considerably larger spread. In the Andersson & Edvardsson (1994) case, the large scatter is due to that their spectra was severely affected by fringing and that many of their spectra had an insufficient S/N to enable good abundance determination from the extremely weak [C I] line. The reason for the large scatter in the Takeda & Honda (2005) data is due to that their spectra in many cases were of low quality

---

[4] Many of the [C/H] values in the Andersson & Edvardsson (1994) data set are only upper limit estimates. These were rejected from the analysis presented here.
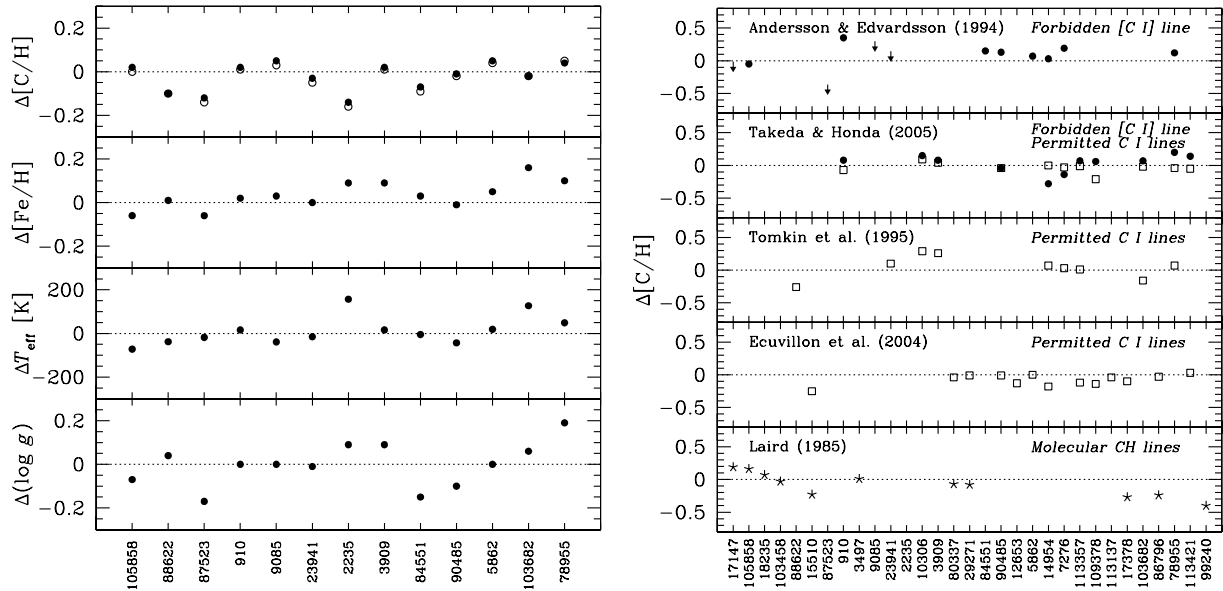
Figure 9. Left-hand panel: a detailed comparison of abundances and stellar parameters for stars that we have in common with Gustafsson et al. (1999). For the $\Delta[C/H]$ comparison, we also include our abundances derived when neglecting the Fe I blend (open circles). On the 'x-axis', we have marked the *Hipparcos* numbers of the stars. The stars have been sorted accorded to their metallicities, [Fe/H] increasing from the left to the right. Right-hand panel: comparison of carbon abundances for stars that we have in common with other studies. The figure shows our [C/H] values minus [C/H] values from the other studies, and comparisons are made both with studies that use the forbidden [C I] line and with studies that use the permitted C I lines and the molecular CH bands (as indicated in the figure). In the case of Andersson & Edvardsson (1994), the arrows mark stars that they only could give an upper estimate on [C/H]. In the case of Takeda & Honda (2005), the different symbols mark [C/H] abundances from the forbidden [C I] line (solid circles) and from the permitted C I lines (open squares). The stars have been sorted accorded to their metallicities, [Fe/H] increasing to the right. On the 'x-axis', we have marked the *Hipparcos* numbers of the stars. Note the different scales on the 'y-axis' in the left- and right-hand plots. The abundances from the different studies have not been adjusted for differences in the stellar parameters.

(Honda, private communication), and in many weak-line cases they decided to adopt the values from the permitted C I lines (average of $\lambda\lambda505.2/538.0$ nm lines) as their final carbon abundance instead (Fig. 8 and equation 5 only include data from the forbidden line).

Thus it appears that it is safe to say that there is a systematic shift between our abundances and those by Gustafsson et al. (1999) since both data sets are individually well defined. Whether this shift is due to the carbon abundances (vertical shift in Fig. 8) or to the Fe abundances (horizontal shift in Fig. 8), a combination of both, or due to that we included the Fe I blend and they did not, will now be investigated by a comparison of individual abundances for stars that we have in common.

The left-hand panel in Fig. 9 shows a detailed comparison for 13 stars that we have in common with Gustafsson et al. (1999). The mean difference in abundances and stellar parameters is (our values minus theirs, the uncertainties represent the one-sigma standard deviations): $\Delta[C/H] = -0.02 \pm 0.07$ dex, $\Delta[C/H]_{NO\,BLEND} = -0.03 \pm 0.07$ dex, $\Delta[Fe/H] = +0.03 \pm 0.06$ dex, $\Delta T_{eff} = +12 \pm 66$ K, $\Delta \log g = -0.00 \pm 0.10$ dex. Overall, the mean differences between our study and Gustafsson et al. (1999) are small for all these parameters. It should be noted that for these stars our inclusion of the Fe I blend has barely any effect on $\Delta[C/H]$. The differences we see in T_{eff} (+12 K) and $\log g$ (0.00 dex) are small and would only translate into $\Delta[C/H] \approx 0.00$ and $\Delta[Fe/H] \approx 0.01$ (see Table 1).

In Fig. 9 (right-hand panel), we also plot the differences between our abundances and those from other works for a total of 31 stars. Comparisons are made to the two other studies that use the forbidden [C I] line (Andersson & Edvardsson 1994; Takeda & Honda 2005) as well as to studies that use the permitted C I lines (Tomkin et al. 1995;

Ecuvillon et al. 2004; Takeda & Honda 2005) and the molecular CH bands (Laird 1985). With Andersson & Edvardsson (1994), we have 12 stars in common, and for four of those they only give upper limit on [C/H]. For the other eight stars, the difference is +0.12 ± 0.12 dex, i.e. quite large and substantially larger than relative to Gustafsson et al. (1999). Takeda & Honda (2005) use both the forbidden and the permitted carbon lines, and we have 11 stars in common. The mean difference between our and their forbidden [C/H] abundances is +0.04 ± 0.14 dex, and to their permitted [C/H] abundances it is −0.03 ± 0.07 dex. With Tomkin et al. (1995), we have nine stars in common and the difference is +0.05 ± 0.18 dex. With Ecuvillon et al. (2004), we have 13 stars in common and the difference is −0.08 ± 0.08 dex. With Laird (1985), we have 11 stars in common and the difference is −0.08 ± 0.19 dex.

We would suggest that if one were to merge our sample with the Gustafsson et al. (1999) sample, one should increase their [Fe/H] by 0.03 dex and decrease their [C/H] by 0.02 dex (or instead adjust our values accordingly). Even though the reason(s) for these shifts is not fully resolved, this would at least bring our and their samples on to a common baseline. Merging our data with the Andersson & Edvardsson (1994) or the Takeda & Honda (2005) samples would introduce a lot of extra scatter and make any interpretation of the observed carbon trends difficult.

Random errors are partly represented by uncertainties in the stellar atmosphere parameters. In Table 1, we list how typical uncertainties in effective temperature, metallicity and surface gravity ($\Delta T_{eff} = +70$ K, $\Delta[Fe/H] = +0.1$ and $\Delta \log g = +0.1$, respectively) effect the derived abundances for three stars (see also discussions in Bensby et al. 2003, 2004).

Random errors may also be due to uncertainties, or defects, in the observed spectra. Here, we paid special attention to features in the spectra that could be leftovers from the reduction procedure and a possible insufficient removal of the fringing pattern. For seven stars (listed in Section 4.3), we did not determine any carbon abundances due to that the [C I] line was severely deformed. For the remaining stars, we could not distinguish any possible fringing residuals from the ever-present random scatter (noise). If the initial fringing pattern affects the final carbon abundances (by an inefficient removal), we would probably see a substantially larger scatter in the carbon trends than what we see in our oxygen trends for which we used the same spectrograph and the same analysis method but for the forbidden [O I] line at 630.0 nm (Bensby et al. 2004). Although a larger scatter indeed seems to be present for the carbon trends than for our oxygen trends, we find that the [C/H] versus [Fe/H] trend is quite well defined (see Fig. 8), and that effects due to residuals from the fringing pattern have been reduced to a level where they most likely do not affect the general appearance of the abundance trends.

Random errors may also arise from errors in the actual fitting of the synthetic spectra to the observed ones. A major concern here is the location of the continuum. Due to the weakness of the [C I] line, a small change in the location of the continuum will have an effect on the carbon abundance. This problem will vary with the quality of the spectra as well as the strengths of the [C I] line and surrounding lines making a true estimate of the uncertainties in the placement of the continuum level difficult. By examining our spectra and varying the continuum level, we estimate an average uncertainty of 0.06 dex in [C/H]. Since the spectra we used in Bensby et al. (2004) did not suffer from fringing effects and generally were of higher quality, we estimate the error in [O/H] to be half of that in [C/H], i.e. 0.03 dex.

Including a random error of 0.06 dex in [C/H] and 0.03 dex in [O/H] due to uncertainties in the continuum level, we estimate that the total random errors in our final [C/H], [C/Fe], [O/H] and [C/O] are 0.07, 0.10, 0.07 and 0.07 dex, respectively (see Table 3).

5 RESULTS AND DISCUSSION

Before we discuss our carbon results and where carbon might be produced, we first, briefly, recap some of the most important features of our sample selection, i.e. the kinematic definition of the two samples. We then turn to a description of the abundance trends found and their implications for where carbon can have formed.

5.1 The kinematic definition of our samples

The stars in our sample were selected, based on their kinematics, to either be typical representatives of the thin or the thick Galactic disc. The kinematic selection is further described in Bensby et al. (2003, 2005) including an extended discussion of how, for example, the local normalization of the thick disc influences the categorization of an individual star.

In Fig. 10(a), we show a so-called Toomre diagram for our stars. The distribution of the stars in our two samples in this plot is essentially the same as Fuhrmann (2004) finds for his thin and thick disc samples. Fig. 10(b) shows the W_{LSR} velocity (which is proportional to the maximum distance below/above the Galactic plane, Z_{max}, a star can reach) as a function of [Fe/H]. We see that even at [Fe/H] = 0 or higher, there are stars with high W_{LSR}. The number of such stars appears to be higher than one would expect from orbital heating by, for example, molecular clouds (Hänninen & Flynn 2002).

One should though remember that our sample is far from complete and we certainly are subject to various biases. However, our point is that these stars do exist, are readily found in any large catalogue (hence not rare objects) and they imply that the thick disc indeed extends to at least solar metallicities.

Finally, it is also worthwhile to note, as pointed out by e.g. Nordström et al. (2004), that there is a lot of kinematic structure when studying large samples of nearby stars. One such structure, or group of stars, of particular interest here is the Hercules stream which has kinematic properties very similar to some of the thick disc stars. Famaey et al. (2005) studied a sample of ~6700 nearby K and M giants and were able to identify several such structures (including the Hercules stream) for which they determined kinematic properties as well as local number densities. From their results, we see that it is especially Hercules stream stars with high U_{LSR} velocities in the direction away from the Galactic centre that could be erroneously classified as thick disc stars. Using a compilation of chemical abundances, Soubiran & Girard (2005) find that the abundance trends for the Hercules stream mostly follow those in the thin disc.

We have checked for possible contamination from Hercules stream in our samples. This was done by recalculating the probabilities that we used when selecting our samples (see Bensby et al. 2003, 2005), and now including the properties for the Hercules stream (see Table 2). Using the same equations as in Bensby et al. (2003, 2005) (but now modified to also include U_{lag} and W_{lag}), we find that none of our stars is more likely to belong to the Hercules stream than to the thin or thick discs.

For the discussion of our carbon results from this paper, we will assume that our stellar samples are representative for the thin and

Table 3. Estimates of the effects on the derived abundances due to errors in the atmosphere parameters. σ_{cont} is the estimated error due to erroneous placement of the continuum (see text) and σ_{tot} is the total random error that were calculated assuming the individual errors to be uncorrelated. The values for O and Fe were taken from Bensby et al. (2004b).

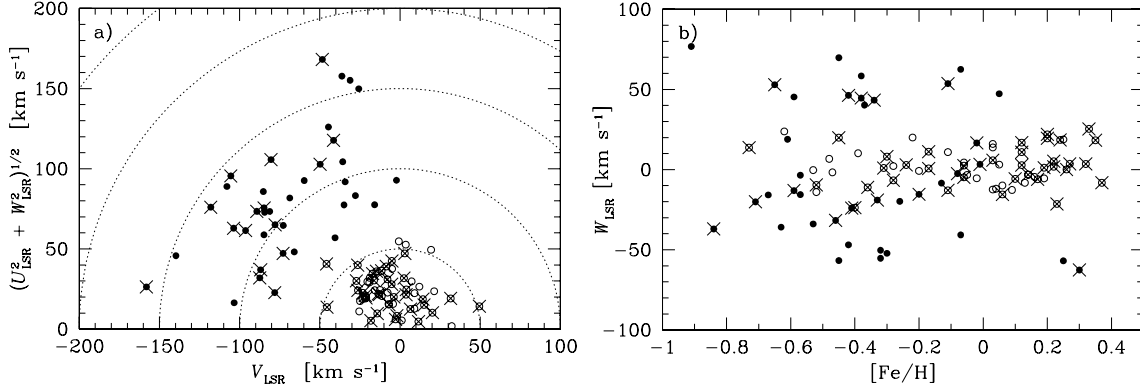|	$\left[\frac{Fe}{H}\right]$	$\left[\frac{O}{H}\right]$	$\left[\frac{O}{Fe}\right]$	$\left[\frac{C}{H}\right]$	$\left[\frac{C}{Fe}\right]$	$\left[\frac{C}{O}\right]$
HIP 88622, (−0.46, 5720, 4.35)						
$\Delta T_{eff} = +70$ K	+0.06	+0.02	−0.04	−0.01	−0.07	−0.03
$\Delta \log g = +0.1$	−0.01	+0.04	+0.05	+0.03	+0.04	−0.01
$\Delta \xi_t = +0.15$ km s^{-1}	−0.02	0.00	+0.02	0.00	+0.02	0.00
Δ[Fe/H] = +0.1	+0.01	+0.03	+0.02	+0.01	0.00	−0.02
σ_{atm}	0.06	0.05	0.07	0.03	0.08	0.04
HIP 82588, (−0.02, 5470, 4.55)						
$\Delta T_{eff} = +70$ K	+0.05	+0.01	−0.04	−0.01	−0.06	−0.02
$\Delta \log g = +0.1$	−0.01	+0.04	+0.05	+0.03	+0.04	−0.01
$\Delta \xi_t = +0.15$ km s^{-1}	−0.03	0.00	+0.03	0.00	+0.03	0.00
Δ[Fe/H] = +0.1	+0.01	+0.04	+0.03	+0.02	+0.01	−0.02
σ_{atm}	0.06	0.06	0.08	0.04	0.08	0.03
HIP 103682, (+0.27, 5940, 4.26)						
$\Delta T_{eff} = +70$ K	+0.05	+0.02	−0.03	0.00	−0.05	−0.02
$\Delta \log g = +0.1$	−0.01	+0.05	+0.06	+0.04	+0.05	−0.01
$\Delta \xi_t = +0.15$ km s^{-1}	−0.05	0.00	+0.05	0.00	+0.05	0.00
Δ[Fe/H] = +0.1	0.00	+0.03	+0.03	+0.01	+0.01	−0.02
σ_{atm}	0.07	0.06	0.09	0.04	0.09	0.03
$\langle \sigma_{atm} \rangle$	0.06	0.06	0.08	0.04	0.08	0.03
σ_{cont}		0.03	0.03	0.06	0.06	0.07
$\langle \sigma_{tot} \rangle$	0.06	0.07	0.09	0.07	0.10	0.07

Figure 10. (a) Toomre diagram; dotted lines indicate constant peculiar space velocities, $v_{pec} = (U_{LSR}^2 + V_{LSR}^2 + W_{LSR}^2)^{1/2}$, in steps of 50 km s^{-1}. (b) W_{LSR} versus [Fe/H]. The plots include our full thin disc (empty circles) and thick disc (filled circles) samples from Bensby et al. (2003, 2005). Those stars that are included in this study are marked by crosses.
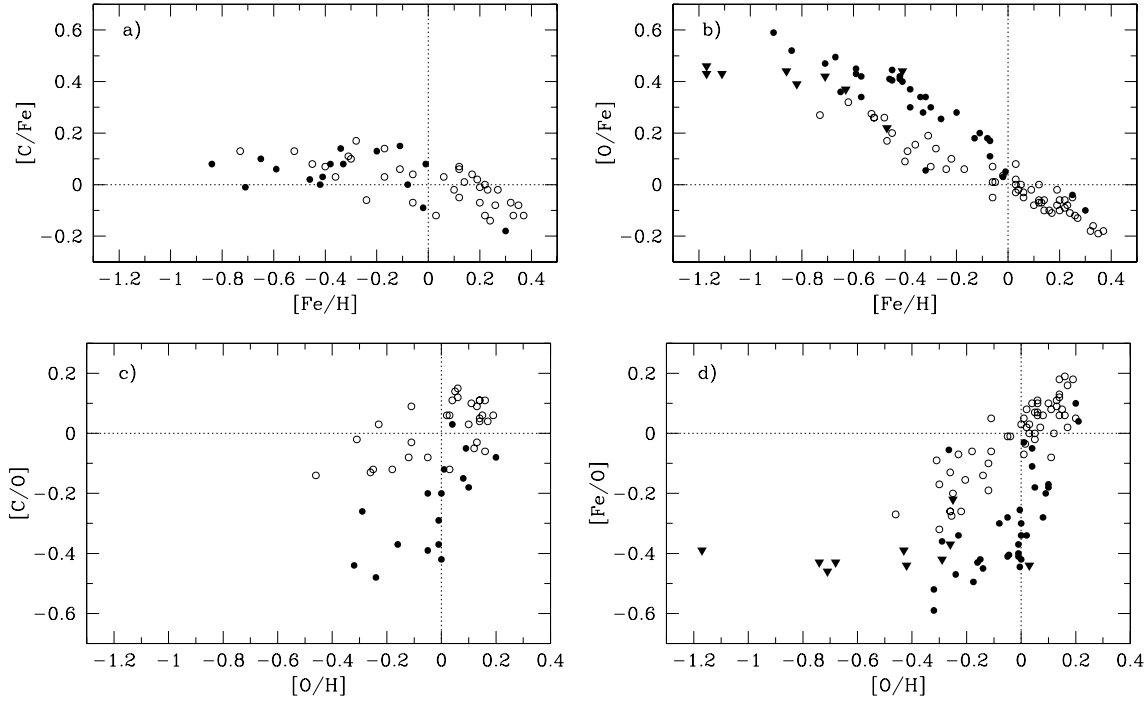

Figure 11. (a) and (b) show the carbon and oxygen abundances, respectively, relative to iron. (c) and (d) show the carbon and iron abundances, respectively, relative to oxygen. All carbon abundances are from this work, and the oxygen and iron abundances have been taken from Bensby et al. (2003, 2004, 2005), see also Table 1. Thin and thick disc stars are marked by open and filled circles, respectively. A few thick disc stars from Nissen et al. (2002) included in the oxygen plots are marked by filled triangles.

thick discs, or the stellar components that can be kinematically associated with the two discs, and that the thick disc does extend up and until solar metallicities.

5.2 Observed trends

5.2.1 [C/Fe] versus [Fe/H]

In Fig. 11(a), we show the trend of [C/Fe] versus [Fe/H]. The thin and thick disc [C/Fe] trends are fully merged and at subsolar metallicities the [C/Fe] values all fall within $0 \lesssim$ [C/Fe] $\lesssim 0.2$ with no particular slope. At super-solar metallicities, the [C/Fe] values decrease with

increasing [Fe/H] [independent of if the Fe I blend is included or not; compare Figs 7(d) and (e)].

The flat [C/Fe] trend that we see at [Fe/H] < 0 is what generally is found, within the uncertainties, in the literature (see e.g. compilation by Gavilán et al. 2005). Gustafsson et al. (1999), however, find an increase in [C/Fe] for decreasing [Fe/H]. This is somewhat discomforting since both our and their carbon abundances are based on the forbidden line at 872.7 nm. However, at a closer look at the [C/Fe] versus [Fe/H] trend in Gustafsson et al. (1999), it is possible that our and their trends are not that different. That they see a slope seem to be mainly based on a few (∼5) stars with [C/Fe] > 0.2 at [Fe/H] $\lesssim -0.6$ (see their fig. 4). So, *if* those stars are disregarded, our and their [C/Fe] versus [Fe/H] trends
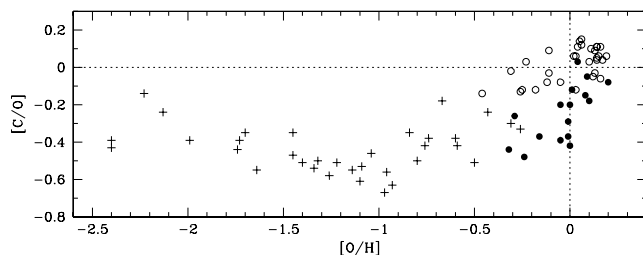
Figure 12. [C/O] versus [O/H]. Our thin and thick disc stars are marked by open and filled circles, respectively. Halo stars from Akerman et al. (2004) are marked by crosses. Note that the Akerman et al. (2004) [C/O] values are overestimated by ∼0.2 dex at the lowest [O/H] due to neglect of NLTE effects. The effect decreases as [O/H] increases.

are, within the uncertainties, similar. Good agreement to Gustafsson et al. (1999) is further strengthened from the detailed comparison in Section 4.5.

5.2.2 [C/O] versus [O/H]

Fig. 11(c) shows the [C/O] versus [O/H] trend for our stellar sample. The thin and thick discs show trends that are clearly separated. The thin disc shows a shallow increase in [C/O] with [O/H] whilst the thick disc first has a flat [C/O] trend that increases sharply at [O/H] = 0. The great resemblance with the observed [Fe/O] versus [O/H] trends shown in Fig. 11(d) could indicate that C and Fe indeed originate from objects that evolve on similar time-scales. As our stellar sample spans a rather limited range in [O/H], it is difficult to use this sample only to say how the [C/O] trend for the thick disc would have evolved from very low oxygen abundances (i.e. [O/H] $\lesssim$ −0.4). In Fig. 12, we therefore show our [C/O] versus [O/H] trend together with the stellar sample (consisting of stars with halo kinematics) from Akerman et al. (2004). They based their carbon and oxygen abundances on permitted C I and O I lines. As they assumed that the non-local thermodynamic equilibrium (NLTE) corrections for the C and O abundances for these lines are of similar size, they did not apply any NLTE corrections. However, recent NLTE calculations by Fabbian et al. (2005) have shown that these 'permitted' [C/H] values should be decreased by as much as ∼0.4 dex at [O/H] $\approx$ −2.3 and less at higher [O/H]. The NLTE corrections for [O/H] are slightly less (−0.1 to −0.3 dex, depending on stellar parameters) resulting in the [C/O] being overestimated by ∼0.2 dex at the lowest [O/H] in the Akerman et al. (2004) data (see also Asplund 2005). As a consequence, the upturn seen in [C/O] with decreasing [O/H] for [O/H] $\lesssim$ −1 in the Akerman et al. (2004) data is overestimated – their trend should be flatter.

Table 4. Kinematic properties of the stellar populations that were used when calculating probabilities to select thin and thick disc stars. The properties of the Hercules stream have been adopted from Famaey et al. (2005), and the properties of the other populations are the same as in Bensby et al. (2005) except for the thin disc that has a lower number density (X) due to the now included Hercules stream. All velocities and velocity dispersions are given in km s^{-1}.

	X	σ_U	σ_V	σ_W	U_{lag}	V_{lag}	W_{lag}
Thin disc	0.84	35	20	16	0	−15	0
Thick disc	0.10	67	38	35	0	−46	0
Hercules	0.06	26	9	17	−40	−50	−7
Halo	0.015	160	90	90	0	−220	0

5.3 Where is carbon made?

The carbon yields for various objects differ significantly. The yields are sensitive to a number of factors, such as stellar winds, treatment of convection and the ^{12}C(α, γ)^{16}O rate. Earlier models of massive stars found them to give high yields of C (e.g. Maeder 1992) whilst these were adjusted downwards once rotation was taken into account (Meynet & Maeder 2002). Several studies have used these yields to model galactic chemical evolution and compare it with observed abundance trends (both in local stars and in Galactic and extra-galactic H II regions). Gustafsson et al. (1999) gave an exhaustive list and discussed the possible sites for carbon. These include supernovae, novae, Wolf–Rayet stars, low- and intermediate-mass stars in the planetary nebula phase or by super-winds at the end or the red-giant phase. Through an analysis of Galactic dwarf stars [a mixture of thin disc stars, metal-poor thick disc stars, as well as stars with intermediate kinematics from Edvardsson et al. (1993)] and data from dwarf galaxies, they arrived at the conclusion that the main contribution of carbon to the galactic chemical evolution comes from super-winds of metal-rich massive stars, that low-mass stars were ruled out and that the role of the intermediate-mass stars remained unclear. Henry et al. (2000) modelled a large set of Galactic and extra-galactic H II regions and reached at a similar conclusion. Other studies find that the low- and intermediate-mass stars are the essential contributors to the chemical enrichment of the Galaxy. By adopting the new yields by Meynet & Maeder (2002), Chiappini et al. (2003b) conclude that massive stars do contribute to the carbon enrichment but that the main contribution at higher metallicities must be due to low- and intermediate-mass stars. Using the same set of yields, Chiappini et al. (2003a) are also able to explain the abundance ratios in other galaxies, such as irregulars. The recent study by Carigi et al. (2005) arrives at a similar complex explanation for the observed abundance patterns where metallicity-dependent yields are necessary both for the massive stars (increasing yields with metallicity) and for low- and intermediate-mass stars (decreasing yields with increasing metallicity). In their best-fitting model, the massive stars dominate the C enrichment at early times, and the low-mass and intermediate-mass stars start to contribute later. The contributions at later times are roughly equal for the two sources. As Carigi et al. (2005) had to invoke the yields by Maeder (1992) [that no longer should be used as they are superseded by Meynet & Maeder (2002)] in order to reproduce the solar [C/O] ratio, the importance they attribute to massive stars at higher metallicities could be overestimated.

Our [C/Fe] versus [Fe/H] trend in the thick disc is flat whilst our [O/Fe] versus [Fe/H] trend [see Figs 11(a) and (b), respectively] shows a clear break and subsequent downturn at [Fe/H] = −0.5 (this corresponds to [O/H] $\approx$ 0). This type of downturn is normally interpreted as the onset of SN Ia (see e.g. Tinsley 1979; Matteucci 2001), and since oxygen is only produced in SN II the increased Fe production by SN Ia results in a downwards trend as [Fe/H] increases. For [C/Fe] versus [Fe/H], we see no such trend. Hence, we may infer from the C abundances in our thick disc sample that enrichment from carbon happens on the same time-scale as the enrichment from SN Ia. Hence, the increase in Fe production is matched by enrichment of C.

The fact that our [C/O]–[O/H] and [Fe/O]–[O/H] trends are indeed very similar further strengthens the importance of low- and intermediate-mass stars as contributors to the carbon enrichment at higher metallicities. This is also supported by Chiappini et al. (2003b), who predict, if low- and intermediate-mass stars are important, that there first would be a flat [C/O] plateau for the thick

disc that then (at roughly solar [O/H]) should sharply increase, to be followed by a shallow thin disc [C/O] trend at higher [C/O] ratios. And this is just what our data show.

Furthermore, Akerman et al. (2004) note that the amplitude of the rise that they see in the [C/O] ratio around [O/H] = −1 in their Milky Way halo stars (see Fig. 12) is well matched by similar trends for H II regions in nearby spiral and irregular galaxies. They this interpret as favourable for their findings that massive stars are the main contributor to the chemical enrichment of carbon as it would be very unlikely that the abundance trends in galaxies that have experienced different types of chemical histories should be so similar if carbon was mainly produced in sites where a substantial time-delay had to be invoked, e.g. low-mass stars. Given the uncertainties relating to NLTE corrections of the Akerman et al. (2004) data (see discussion above) and that Chiappini et al. (2003a) are able to explain the abundance ratios in other galaxies as well (including irregulars), using the same set of yields that were used for the Milky Way, this indicates that the role of massive stars might be overestimated by Akerman et al. (2004).

If we compare our C abundances with Y, the trend of [C/Y] versus [Y/H] shows a flat trend for [Y/H] $\lesssim$ 0 which turns to a steadily declining trend for [Y/H] $\gtrsim$ 0 [see Fig. 13(a)] which is very similar to what we see for [C/Fe] versus [Fe/H] [see Fig. 11(a)]. [C/Y] versus [Fe/H] is somewhat different, being, essentially, flat for both the thin and the thick disc samples at all metallicities [see Fig. 13(b)]. Approximately 70 per cent of Y are produced in the s-process in asymptotic giant branch (AGB) stars and ∼30 per cent come from massive stars (∼10 per cent from a weak 'secondary' s-process component and ∼20 per cent from a primary component; Travaglio et al. 2004). The most straightforward interpretation of the lack of trends would be that the two elements, C and Y, are made in objects that enrich the interstellar medium on the same time-scale. Most naively, we would assume that their major components are indeed made in the same objects, namely low- and intermediate-mass stars in the AGB phase. However, if we inspect the trend of [C/Y] versus

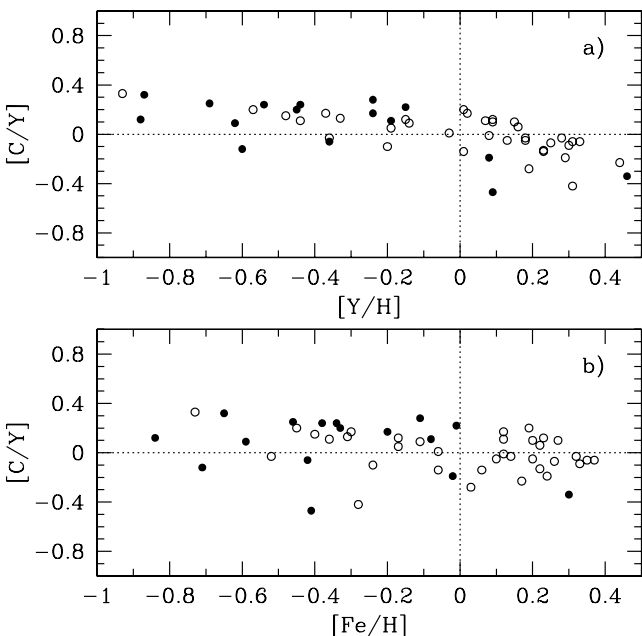[Y/H] in addition to the flat trend below subsolar [Y/H] we see a declining trend of [C/Y] for [Y/H] > 0 indicating that as the Y increases there is a decrease in C production. This could be due to a metallicity effect in the production of s-process elements that favours light s-process elements (such as Y) over heavy s-process elements (such as Ba) at high metallicities (Busso et al. 2001; Bensby et al. 2005).

So, we have shown that the carbon production must balance the Fe production by SN Ia and the Y production by AGB stars. With this observable in mind, it appears that either the massive stars must have (very) metallicity-dependent yields that are finely tuned to the [Fe/H] time-scale of SN Ia as observed in the Milky Way thick disc or less massive stars are significant contributors too.

In summary, we thus find that the carbon enrichment at low metallicities (i.e. the Galactic halo and metal-poor thick disc) is due to massive stars, but as more and more low- and intermediate-mass stars start to contribute to the general enrichment they also more and more dominate the carbon enrichment of the interstellar medium as it is seen in the thin disc and the metal-rich thick disc.

6 SUMMARY

We present carbon abundances in 51 F and G dwarf stars (16 thick disc stars and 35 thin disc stars) in the solar neighbourhood. The analysis is based on the forbidden [C I] line at 872.7 nm which is an abundance indicator that is insensitive to errors in the stellar atmosphere parameters. Combining these data with our previously published oxygen abundances, based on the forbidden [O I] line at 630.0 nm (see Bensby et al. 2004), we can form very robust [C/O] ratios that we then used to investigate the origin of carbon and the chemical evolution of the Galactic thin and thick discs. Our findings concerning carbon abundance trends in the Galactic thin and thick discs include the following.

(i) At subsolar [Fe/H], we find that the [C/Fe] versus [Fe/H] trends for the thin and thick discs are fully merged and essentially flat. For the thin disc, that extends to higher metallicities, [C/Fe] is flat until [Fe/H] = 0 when a slow decline starts [see Fig. 11(a)].

(ii) Our abundance trends indicate that the sources that contribute to the carbon enrichment of the interstellar medium do so on the same time-scale as those that produce most of the iron, i.e. SN Ia. The production of C and Y (coming mainly from AGB stars) also seems to work on the same time-scale.

(iii) In light of our own as well as other studies in the literature (notably Gustafsson et al. 1999; Chiappini et al. 2003a,b; Akerman et al. 2004; Carigi et al. 2005), we feel that the source(s) of carbon is not yet settled but that there is growing evidence that a complicated, and finely tuned, set of objects contributes to the enrichment of carbon in galaxies. As discussed, based on our own results only, we would conclude that the main source for carbon in the Galaxy is low- and intermediate-mass stars. However, for the Milky Way galaxy it appears that massive stars played a significant role for the carbon enrichment at low metallicities (i.e. halo and metal-poor thick disc) whereas low- and intermediate-mass stars dominate more and more at higher metallicities, i.e. that they have been the major contributors to the carbon enrichment in the thin disc and the metal-rich thick disc.

From our analysis of the forbidden [C I] line at 872.7 nm to determine carbon abundances in solar-type stars, we also found a few details that we think are noteworthy. (1) By examining how the neglect of the blending Fe I line affects the derived carbon abundances from the forbidden [C I] line, we find that it is mainly for

Figure 13. (a) [C/Y] versus [Y/H] and (b) [C/Y] versus [Fe/H]. Yttrium abundances are taken from Bensby et al. (2005). Thin and thick disc stars are marked by open and filled circles, respectively.

stars with effective temperatures less than ∼5700 K that differences are large [see Fig. 7(a)]. (2) Currently, the only available source for the oscillator strength of the blending Fe I line is a theoretical one (Kurucz 1993). Therefore, it is possible that the strength of the Fe I could be under- or overestimated. By working strictly relative to the Sun, the effects of an erroneous treatment of the blend will be reduced. *It would, however, be very valuable if a* log gf *-value for the Fe* I *line could be measured in the laboratory.* (3) For the Sun we find a carbon abundance of $\epsilon_\odot(C) = 8.41$ when including the Fe I blend and $\epsilon_\odot(C) = 8.44$ when neglecting it. (4) The general appearance of our carbon trends in the two discs is similar whether we include the Fe I blend in the abundance analysis or not [see Figs 7(d) and (e)].

ACKNOWLEDGMENTS

REFERENCES

Akerman C. J., Carigi L., Nissen P. E., Pettini M., Asplund M., 2004, A&A, 414, 931
Allende Prieto C., Lambert D. L., Asplund M., 2002, ApJ, 573, L137
Andersson H., Edvardsson B., 1994, A&A, 290, 590
Arnett D., 2004, in McWilliam A., Rauch M., eds, Carnegie Observatories Astrophys. Ser. Vol. 4, Origin and Evolution of the Elements. Cambridge Univ. Press, Cambridge, p. 12
Asplund M., 2005, ARA&A, 43, 481
Asplund M., Gustafsson B., Kiselman D., Eriksson K., 1997, A&A, 318, 521
Asplund M., Grevesse N., Sauval A. J., Allende Prieto C., Blomme R., 2005, A&A, 431, 693
Barklem P. S., O'Mara B. J., Ross J. E., 1998, MNRAS, 296, 1057
Bensby T., Feltzing S., Lundström I., 2003, A&A, 410, 527
Bensby T., Feltzing S., Lundström I., 2004, A&A, 415, 155
Bensby T., Feltzing S., Lundström I., Ilyin I., 2005, A&A, 433, 185
Busso M., Gallino R., Lambert D. L., Travaglio C., Smith V. V., 2001, ApJ, 557, 802
Carigi L., Peimbert M., Esteban C., García-Rojas J., 2005, ApJ, 623, 213
Chiappini C., Romano D., Matteucci F., 2003a, MNRAS, 339, 63
Chiappini C., Matteucci F., Meynet G., 2003b, A&A, 410, 257
Ecuvillon A., Israelian G., Santos N. C., Mayor M., Villar V., Bihain G., 2004, A&A, 426, 619
Edvardsson B., Andersen J., Gustafsson B., Lambert D. L., Nissen P. E., Tomkin J., 1993, A&A, 275, 101
Fabbian D., Asplund M., Carlsson M., Kiselman D., 2005, in Hill V., Francois P., Primes F., eds, Proc. IAU Symp. 228, From Li to U: Elemental Tracers of Early Chemical Evolution. Cambridge Univ. Press, Cambridge, p. 225
Famaey B., Jorissen A., Luri X., Mayor M., Udry S., Dejonghe H., Turon C., 2005, A&A, 430, 165
Fuhrmann K., 2004, Astron. Nachr., 325, 3
Galavis M. E., Mendoza C., Zeippen C. J., 1997, A&AS, 123, 159
Gavilán M., Buell J. F., Mollá M., 2005, A&A, 432, 861
Gray D. F., 1992, The Observation and Analysis of Stellar Photospheres, 2nd edn. Cambridge Astrophysics Series. Cambridge Univ. Press, Cambridge
Gustafsson B., Bell R. A., Eriksson K., Nordlund A., 1975, A&A, 42, 407
Gustafsson B., Karlsson T., Olsson E., Edvardsson B., Ryde N., 1999, A&A, 342, 426
Hänninen J., Flynn C., 2002, MNRAS, 337, 731
Henry R. B. C., Kwitter K. B., Bates J. A., 2000, ApJ, 531, 928
Hibbert A., Biemont E., Godefroid M., Vaeck N., 1993, A&AS, 99, 179
Kupka F., Piskunov N., Ryabchikova T. A., Stempels H. C., Weiss W. W., 1999, A&AS, 138, 119
Kurucz R., 1993, SYNTHE Spectrum Synthesis Programs and Line Data. Kurucz CD-ROM No. 18. Smithsonian Astrophysical Observatory, Cambridge, MA, 18
Laird J. B., 1985, ApJ, 289, 556
Lambert D. L., Swings J. P., 1967, Solar Phys., 2, 34
Lambert D. L., Ries L. M., 1977, ApJ, 217, 508
Liang Y. C., Zhao G., Shi J. R., 2001, A&A, 374, 936
Maeder A., 1992, A&A, 264, 105
Matteucci F., 2001, The Chemical Evolution of the Galaxy. Astrophysics and Space Science Library. Vol. 253, Kluwer Academic Publishers, Dordrecht
Meynet G., Maeder A., 2002, A&A, 390, 561
Nissen P. E., Primas F., Asplund M., Lambert D. L., 2002, A&A, 390, 235
Nordström B. et al., 2004, A&A, 418, 989
Piskunov N. E., Kupka F., Ryabchikova T. A., Weiss W. W., Jeffery C. S., 1995, A&AS, 112, 525
Ryabchikova T., Piskunov N., Stempels H., Kupka F., Weiss W., 1999, Phys. Scr., T83, 162
Shi J. R., Zhao G., Chen Y. Q., 2002, A&A, 381, 982
Soubiran C., Girard P., 2005, A&A, 438, 139
Takeda Y., Honda S., 2005, PASJ, 57, 65
Tinsley B. M., 1979, ApJ, 229, 1046
Tomkin J., Woolf V. M., Lambert D. L., Lemke M., 1995, AJ, 109, 2204
Travaglio C., Gallino R., Arnone E., Cowan J., Jordan F., Sneden C., 2004, ApJ, 601, 864
Wallerstein G. et al., 1997, Rev. Mod. Phys., 69, 995

This paper has been typeset from a TEX/LATEX file prepared by the author.